Reboul, J. y Vadillo, G. (2018). Homogenized Gurson-type behavior equations for strain rate sensitive materials. *Acta Mechanica*, 229(8), pp. 3517–3536.

DOI: https://doi.org/10.1007/s00707-018-2189-0

J. Reboul · G. Vadillo

Homogenized Gurson-type behavior equations for strain rate sensitive materials

Abstract In this paper, the classical Gurson model for ductile porous media is extended for strain-rate-dependent materials. Based on micromechanical considerations, approximate closed-form macroscopic behav-ior equations are derived to describe the viscous response of a ductile metallic material. To this end, the analysis of the expansion of a long cylindrical void in an ideally plastic solid introduced by McClintock (J Appl Mech 35:363, 1968) is revisited. The classical Gurson yield locus has been modified to explicitly take into account the strain rate sensitivity parameter for strain rate power-law solids. Two macroscopic approaches are proposed in this work. Both models use the first term of a Taylor series expansion to approximate integrals to polynomial functions. The first proposed closed-form approach is analytically more tractable than the second one. The second approach is more accurate. In order to compare the proposed approximate Gurson-type macroscopic functions with the behavior of the original Gurson yield locus, numerical finite element analyses for cylindrical cells have been conducted for a wide range of porosities, triaxialities, and strain rate sensitivity parameters. The results presented evidence that, for large values of the rate sensitivity parameters, the proposed extended Gurson-type models have the important quality to better predict the behavior of rate sensitive materials than the classical one. They also provide simpler and accurate alternatives to more traditional viscoplastic models.

1 Introduction

The process of fracture in the form of evolving crack surfaces in ductile solid materials is preceded by significant plastic deformations. Prediction of failure mechanisms due to void initiation and growth is an intriguingly challenging task and plays an extremely important role in various engineering applications like cutting, machining, metal forming, and high-speed impact.

The early analyses by McClintock [1] and Rice and Tracey [2] based on the growth of cylindrical or spherical voids in ductile matrices have provided the basis for numerous studies on the micromechanics of porous plastic solids. Distinct features of these models are that voids are explicitly taken into account, and precise constitutive models for characterization of the void-containing material behavior are used. The most widely known is that originally introduced by Gurson [3]. Gurson's analysis proposed a macroscopic yield criterion for a rigid plastic isotropic matrix containing either a cylindrical or a spherical void and considers the solid matrix obeying the von Mises criterion.

Over the past three decades, various extensions of the Gurson model have been developed and provided to better represent the response of ductile metals: void nucleation and coalescence [4,5], void shape effects [6–9], strain hardening [10], plastic anisotropy of the matrix material [11–13], influence of the third stress invariant

J. Reboul · G. Vadillo (✉)
Department of Continuum Mechanics and Structural Analysis, University Carlos III of Madrid, Avda. de la Universidad, 30, 28911 Leganés, Madrid, Spain
E-mail: gvadillo@ing.uc3m.es
Tel.: +34916248460
Fax: +34 916249430

in the yielding of porous materials [14,15], etc. For viscoplastic solids, one of the most largely employed modifications of the Gurson model is the one that replaces, in the yield criteria, the constant σ_0 with the relation $\sigma_0\left(\dot{\bar{\varepsilon}}\right)$. The $\sigma_0\left(\dot{\bar{\varepsilon}}\right)$ relation gives the dependence of the equivalent stress of the matrix solid as function of the effective plastic strain rate $\dot{\bar{\varepsilon}}$.

Reliable modeling of the damage process in viscoplastic ductile materials is of paramount importance for many scientific and engineering applications. In order to analyze the homogenized response of porous materials with a Bingham viscoplastic matrix, Perrin [16] obtained, following Rice and Tracey's [2] and Gurson's [3] approaches, explicit expressions of the macroscopic potentials for the case of cylindrical and spherical voids. For viscoplastic power-law materials, methods based on variational principles have been proposed by [17–19] among others. The predictions generated by these variational models have been found to be quite good for low to moderate stress triaxialities. At high stress triaxialities, by contrast, variational models become progressively less accurate than Gurson models, leading to unrealistic predictions for pressure-dominated processes. A general improvement along these lines has been introduced by Danas et al. [20] and Idiart [21].

Various generalizations of the theory of Gurson [3] have been also developed by several authors [22,23] in order to include the effects of power-law viscoplasticity. These Gurson-type approaches, from a practical point of view, mostly require significant computational costs with implementation complexity. The original key contribution of this paper is to overcome this drawback.

Based on first principles, the main effort in this work has been concentrated to provide, for the entire range of positive stress triaxialities and using only material-independent parameters, accurate and simple Gurson-type ductile damage models to correctly describe the ductile behavior of strain rate sensitive materials.

The structure of this article is organized as follows: in Sect. 2, we outline the ductile fracture model of McClintock [1] by the growth of a cylindrical hole. This description serves as the basis for the formulation of the new damage plasticity model. Next, in Sect. 3, new extensions of the Gurson damage model have been proposed for strain-rate-dependent materials. For that task, two different explicit closed-form approximate macroscopic behavior equations are developed for a wide range of stress states and porosities. In Sect. 4, the accuracy of the developed models is assessed by comparison with numerical results using the original Gurson model in finite element cell calculations. Comparisons with Leblond et al. [22] viscoplastic model's results are also presented. Finally, the main conclusions and remarks are given in Sect. 5.

2 Problem formulation

Let us consider a cylindrical cell containing a single cylindrical void, thus representing a material with a periodic array of voids. The material of the cell obeys the theory of J_2 plasticity. The initial height of the cell is H_0, and the initial inner and outer radius is a_0 and b_0, respectively (see Fig. 1). The void grows as remote axisymmetric loadings are applied to the cell. It is assumed that both the cell and the void remain cylindrical throughout the entire growth process.

If generalized plane strain and cylindrical symmetry are assumed, with polar coordinates (r, θ, z), all field quantities are functions solely of the radius r.

- With no body force, the equilibrium equation in cylindrical coordinates is given by:

$$\frac{\mathrm{d}\sigma_r}{\mathrm{d}r} + \frac{\sigma_r - \sigma_\theta}{r} = 0. \tag{1}$$

- The radial displacement $u(r)$ is the only non-vanishing in-plane displacement. The strain rates $(\dot{\varepsilon}_r, \dot{\varepsilon}_\theta, \dot{\varepsilon}_z)$ relations are then given by:

$$\dot{\varepsilon}_r = \frac{\mathrm{d}\dot{u}}{\mathrm{d}r}; \quad \dot{\varepsilon}_\theta = \frac{\dot{u}}{r}; \quad \dot{\varepsilon}_z = \dot{E}_3, \tag{2}$$

  being $\dot{E}_3 = \frac{\dot{H}}{H}$ the rate of macroscopic logarithmic principal strain in x_3 direction.
- Imposing incompressibility condition of the matrix material:

$$\dot{\varepsilon}_r + \dot{\varepsilon}_\theta + \dot{\varepsilon}_z = 0. \tag{3}$$

- The Mises associated flow rule reads:

$$\sigma_r' = \frac{2}{3}\frac{\bar{\sigma}}{\dot{\bar{\varepsilon}}}\,\dot{\varepsilon}_r; \qquad \sigma_\theta' = \frac{2}{3}\frac{\bar{\sigma}}{\dot{\bar{\varepsilon}}}\,\dot{\varepsilon}_\theta; \qquad \sigma_z' = \frac{2}{3}\frac{\bar{\sigma}}{\dot{\bar{\varepsilon}}}\,\dot{\varepsilon}_z, \tag{4}$$

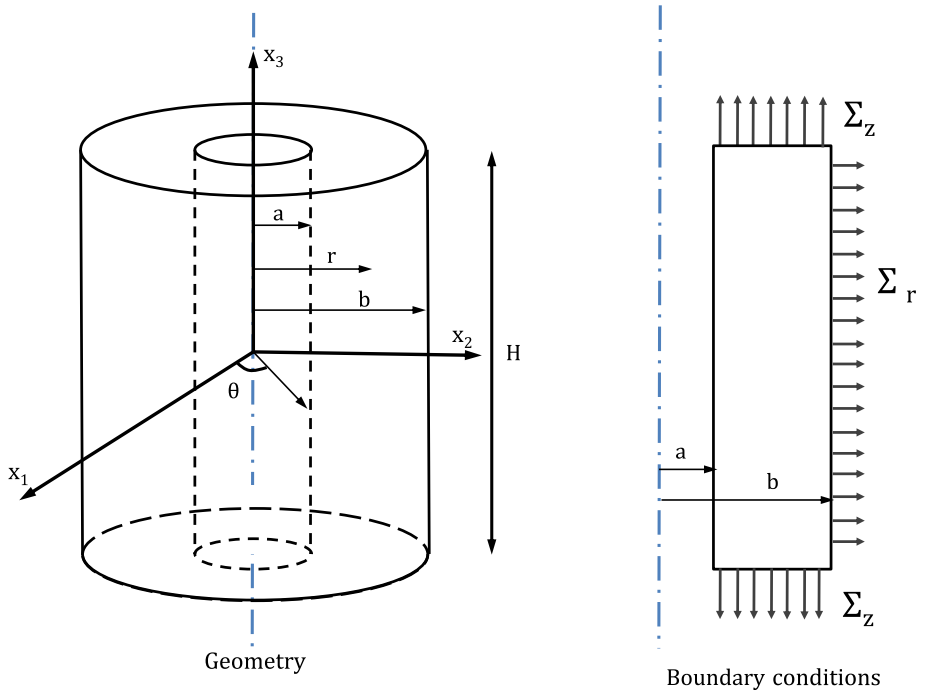

Fig. 1 Simplified representation of a unit cylindrical cell. Geometric parameters and boundary conditions are also presented

being σ_r', σ_θ', σ_z' the deviatoric local stress components with the expressions:

$$\sigma_r' = \sigma_r - \sigma; \qquad \sigma_\theta' = \sigma_\theta - \sigma; \qquad \sigma_z' = \sigma_z - \sigma; \qquad \sigma = \frac{1}{3}\left(\sigma_r + \sigma_\theta + \sigma_z\right), \tag{5}$$

and $\bar{\sigma}$ and $\dot{\bar{\varepsilon}}$ the matrix Mises equivalent stress and the matrix Mises equivalent strain rate, respectively:

$$\bar{\sigma} = \bar{\sigma}\left(\dot{\bar{\varepsilon}}\right); \quad \dot{\bar{\varepsilon}} = \sqrt{\frac{2}{3}\left(\dot{\varepsilon}_r^2 + \dot{\varepsilon}_\theta^2 + \dot{\varepsilon}_z^2\right)}; \quad \bar{\sigma} = \sqrt{\frac{3}{2}\left(\sigma_r'^2 + \sigma_\theta'^2 + \sigma_z'^2\right)}. \tag{6}$$

- Imposing boundary conditions to ensure that the radial stress vanishes at the void surface and remote axisymmetric loadings are prescribed on its external surface yields:

$$\sigma_r(a) = 0, \qquad \sigma_r(b) = \Sigma_r, \qquad \sigma_z(\pm H/2) = \Sigma_z, \tag{7}$$

representing Σ_r, Σ_z the macro average stress, and σ_r, σ_z the local stress of the matrix material, with the relations:

$$\Sigma_1 = \Sigma_2 = \Sigma_r = \frac{1}{V}\int_V \sigma_r \mathrm{d}V; \qquad \Sigma_3 = \Sigma_z = \frac{1}{V}\int_V \sigma_z \mathrm{d}V. \tag{8}$$

The effective stress Σ_{eq} expressed in terms of the macroscopic average stresses in principal directions Σ_1, Σ_2, and Σ_3 ($\Sigma_3 > \Sigma_1 = \Sigma_2$) is:

$$\Sigma_{\mathrm{eq}} = \Sigma_3 - \Sigma_1. \tag{9}$$

To obtain the radial velocity field $\dot{u}(r)$ and the strain rates ($\dot{\varepsilon}_r,\ \dot{\varepsilon}_\theta,\ \dot{\varepsilon}_z$) expressions, the equation of matrix incompressibility (Eq. 3) should be solved imposing boundary conditions, then:

$$\dot{u}(r) = -\frac{\dot{E}_3}{2}r + \frac{A}{r}, \tag{10}$$

$$\dot{\varepsilon}_r = -\frac{\dot{E}_3}{2} - \frac{A}{r^2}, \tag{11}$$

$$\dot{\varepsilon}_\theta = -\frac{\dot{E}_3}{2} + \frac{A}{r^2}, \tag{12}$$

$$\dot{\varepsilon}_z = \dot{E}_3 \tag{13}$$

being the effective strain rate:

$$\dot{\bar{\varepsilon}} = \dot{E}_3 \left(1 + \alpha^2 \left(\frac{a}{r}\right)^4\right)^{1/2}, \tag{14}$$

and A and α:

$$A = -\frac{a^2}{2}\frac{\dot{V}_{\text{void}}}{V_{\text{void}}}; \quad \alpha = \frac{2}{\sqrt{3}}\frac{|A|}{\dot{E}_3 a^2} \tag{15}$$

where a is the current radius of the void, and V_{void} and $\dot{V}_{\text{void}}$ the void volume ($V_{\text{void}} = \pi a^2 H$) and the void volume rate of the cell, respectively.

With the above expressions, the components of the deviatoric stresses of Eq. (4) can be expressed as:

$$\begin{aligned}
\sigma_r' &= \frac{2}{3}\cdot\frac{\bar{\sigma}}{\dot{E}_3\left[1+\alpha^2\left(\frac{a}{r}\right)^4\right]^{1/2}}\cdot\left(-\frac{\dot{E}_3}{2}-\frac{A}{r^2}\right),\\
\sigma_\theta' &= \frac{2}{3}\cdot\frac{\bar{\sigma}}{\dot{E}_3\left[1+\alpha^2\left(\frac{a}{r}\right)^4\right]^{1/2}}\cdot\left(-\frac{\dot{E}_3}{2}+\frac{A}{r^2}\right),\\
\sigma_z' &= \frac{2}{3}\cdot\frac{\bar{\sigma}}{\left[1+\alpha^2\left(\frac{a}{r}\right)^4\right]^{1/2}}.
\end{aligned} \tag{16}$$

The boundary traction conditions on the outer and inner radial surfaces of the cell (Eqs. (7) and (8)) are specified by $\sigma_r(a) = 0,\ \sigma_r(b) = \Sigma_1$. The principal components of the macroscopic stress tensor, Σ_1 and Σ_{eq}, are obtained by integrating σ_r, σ_θ and σ_z along the internal and external cell such that:

$$\Sigma_1 = \sigma_r(b) - \sigma_r(a) = \int_a^b \frac{\mathrm{d}\sigma_r}{\mathrm{d}r}\mathrm{d}r = \int_a^b \frac{\sigma_\theta - \sigma_r}{r}\mathrm{d}r = \int_a^b \frac{\sigma_\theta' - \sigma_r'}{r}\mathrm{d}r, \tag{17}$$

$$\Sigma_{\text{eq}} = \Sigma_3 - \Sigma_1 = \frac{1}{V}\int_V \sigma_z \mathrm{d}V - \frac{1}{V}\int_V \frac{1}{2}\left(\sigma_r + \sigma_\theta\right)\mathrm{d}V = \frac{1}{V}\int_V \left(\sigma_z' - \frac{\sigma_r' + \sigma_\theta'}{2}\right)\mathrm{d}V \tag{18}$$

or equivalently:

$$\Sigma_1 = \frac{4}{3}\int_a^b \frac{\bar{\sigma}}{\dot{E}_3\left[1+\alpha^2\left(\frac{a}{r}\right)^4\right]^{1/2}}\cdot\frac{A}{r^3}\mathrm{d}r, \tag{19}$$

$$\Sigma_{\text{eq}} = \frac{2}{b^2}\int_a^b \frac{\bar{\sigma}}{\left[1+\alpha^2\left(\frac{a}{r}\right)^4\right]^{1/2}}\cdot r\mathrm{d}r. \tag{20}$$

With the change of variable defined by:

$$x = \alpha\left(\frac{a}{r}\right)^2, \tag{21}$$

Equations (19) and (20) become:

$$\Sigma_1 = -\frac{\sqrt{3}}{3}\int_{\alpha}^{f\cdot\alpha}\frac{\bar{\sigma}}{\left(1+x^2\right)^{1/2}}\mathrm{d}x, \tag{22}$$

$$\Sigma_{\mathrm{eq}} = -f\cdot\alpha\int_{\alpha}^{f\cdot\alpha}\frac{\bar{\sigma}}{x^2\left(1+x^2\right)^{1/2}}\mathrm{d}x. \tag{23}$$

being $f = \left(\frac{a}{b}\right)^2$.

The macroscopic function Φ, that is dependent of macroscopic strain rates and stresses, will be obtained by the integration and combination (where α is removed from the formulation) of the above two mentioned equations.

2.1 Rate-independent material case

In the particular case where the matrix material is strain rate independent, the equivalent stress is given by the formula:

$$\bar{\sigma} = \sigma_0 \tag{24}$$

with σ_0 a reference yield stress. Calculation of Σ_1, Σ_{eq}, from Eqs. (22, 23), yields:

$$\Sigma_1 = -\frac{\sigma_0}{\sqrt{3}}\int_{\alpha}^{f\cdot\alpha}\frac{\mathrm{d}x}{\left(1+x^2\right)^{1/2}} = \frac{\sigma_0}{\sqrt{3}}\,\mathrm{Ln}\left(\frac{\alpha+\sqrt{1+\alpha^2}}{f\cdot\alpha+\sqrt{1+(f\cdot\alpha)^2}}\right), \tag{25}$$

$$\Sigma_{\mathrm{eq}} = -f\cdot\alpha\cdot\sigma_0\int_{\alpha}^{f\cdot\alpha}\frac{\mathrm{d}x}{x^2\left(1+x^2\right)^{1/2}} = \sigma_0\left(\sqrt{1+(f\cdot\alpha)^2}-f\sqrt{1+\alpha^2}\right). \tag{26}$$

If Eq. (25) is inserted into Eq. (26) in order to remove α, the flow potential for a porous plastic rate-independent material can be written as the well-known form:

$$\Phi = \frac{\Sigma_{\mathrm{eq}}^2}{\sigma_0^2} + 2\,f\cosh\left(\frac{\sqrt{3}\,\Sigma_1}{\sigma_0}\right) - (1+f^2) = 0 \tag{27}$$

which is Gurson's criterion for cylindrical voids.

2.2 Rate-dependent material case

For the sake of simplicity, for a rate-dependent material, the Mises stress $\bar{\sigma}$ is defined by a power-type hardening formulation as:

$$\bar{\sigma} = \sigma_0\left(\dot{\bar{\varepsilon}}\right)^m, \tag{28}$$

being m the strain rate sensitivity parameter and σ_0 a reference value (with units $Pa\cdot s^m$). Equations (19) and (20) become in this case:

$$\frac{\Sigma_1}{\sigma_0\cdot\left(\dot{E}_{\mathrm{eq}}\right)^m} = \frac{\sqrt{3}}{3}\frac{1}{\left(1-\frac{f\cdot\alpha}{\sqrt{3}}\right)^m}\int_{f\cdot\alpha}^{\alpha}\left(1+x^2\right)^{\frac{m-1}{2}}\mathrm{d}x, \tag{29}$$

$$\frac{\Sigma_{\mathrm{eq}}}{\sigma_0\cdot\left(\dot{E}_{\mathrm{eq}}\right)^m} = \frac{f\cdot\alpha}{\left(1-\frac{f\cdot\alpha}{\sqrt{3}}\right)^m}\int_{f\cdot\alpha}^{\alpha}\frac{\left(1+x^2\right)^{\frac{m-1}{2}}}{x^2}\mathrm{d}x, \tag{30}$$

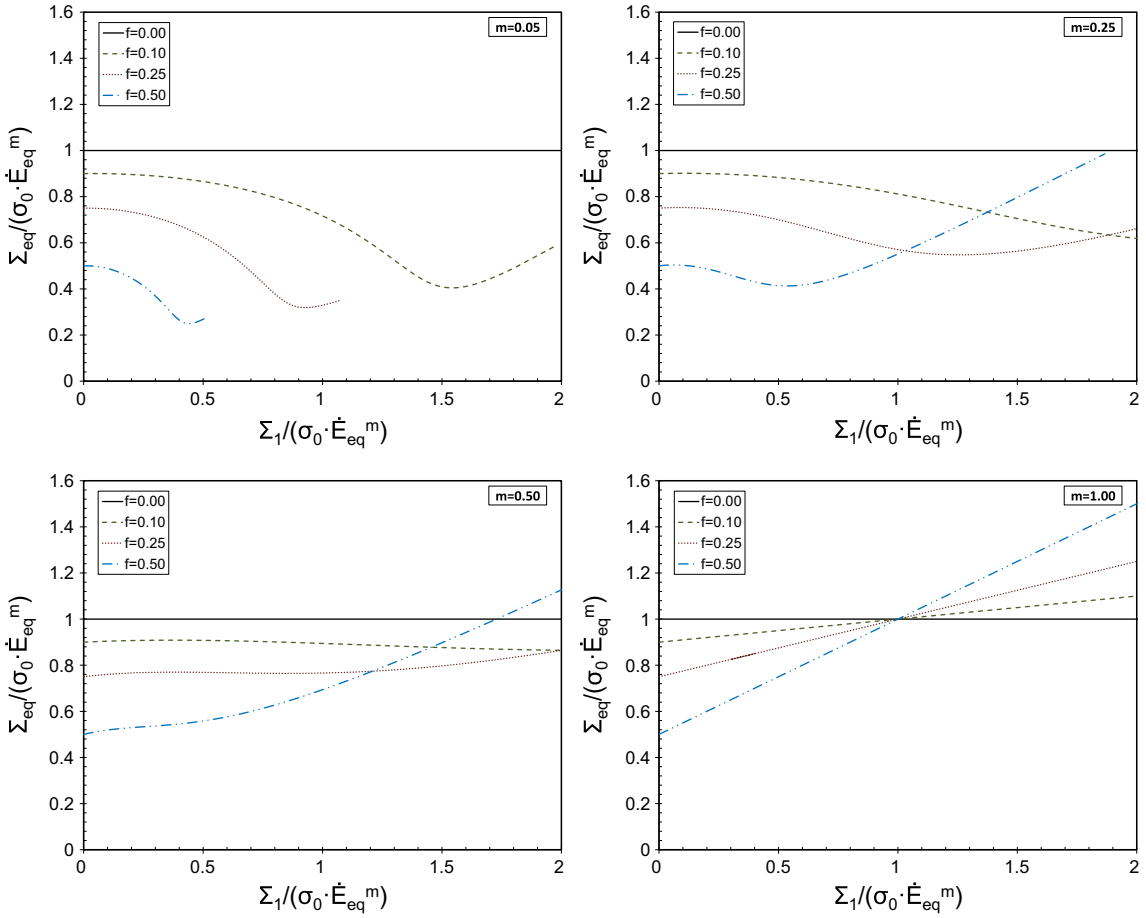

Fig. 2 Exact representation of the relations $\Sigma_1/(\sigma_0(\dot{E}_{\text{eq}})^m) - \Sigma_{\text{eq}}/(\sigma_0(\dot{E}_{\text{eq}})^m)$ (obtained by numerical evaluation) for cylindrical voids with porosities $f = 0.0$, 0.1, 0.25, and 0.5. The strain rate sensitivity parameters considered are $m = 0.05$ (**a**), 0.25 (**b**), 0.5 (**c**), and 1.0 (**d**)

with $\dot{E}_{\text{eq}}$ taking into account incompressibility of the matrix material:

$$\dot{E}_{\text{eq}} = \frac{2}{3}\left(\dot{E}_3 - \dot{E}_1\right) = \dot{E}_3\left(1 - \frac{f\cdot\alpha}{\sqrt{3}}\right). \tag{31}$$

According to the numerical computation of the integrals (Eqs. (29, 30)), a graphical representation of both equations in the $\Sigma_1/\left(\sigma_0\left(\dot{E}_{\text{eq}}\right)^m\right) - \Sigma_{\text{eq}}/\left(\sigma_0\left(\dot{E}_{\text{eq}}\right)^m\right)$ space is presented in Fig. 2. Different values of porosity f and strain rate sensitivity parameter m have been considered. The results show an important effect of the m parameter on the value of the macroscopic surface. The $\Sigma_1/\left(\sigma_0\left(\dot{E}_{\text{eq}}\right)^m\right) - \Sigma_{\text{eq}}/\left(\sigma_0\left(\dot{E}_{\text{eq}}\right)^m\right)$ surface is larger when the m value is higher. The change of shape in the surface is a consequence of the term $\sigma_0\left(\dot{E}_{\text{eq}}\right)^m$ that divides Σ_1 and Σ_{eq} introduced to define dimensionless stress variables. This does not in any way mean a loss of convexity of the flow potential in the macroscopic stress space.

The exact analytical solution of Eqs. (29), (30), to the best of our knowledge, does not exist if $m \neq 0, 1$. In this work, various approximations are made in order to give accurate approximate solutions of the homogenized behavior equations for rate sensitive materials.

3 Analytical approach for the macroscopic behavior of the material

In order to explore the role played by material rate sensitivity in the response of the cylindrical shell, in forthcoming Sections, we will explore, by making various mathematical assumptions and based on Taylor

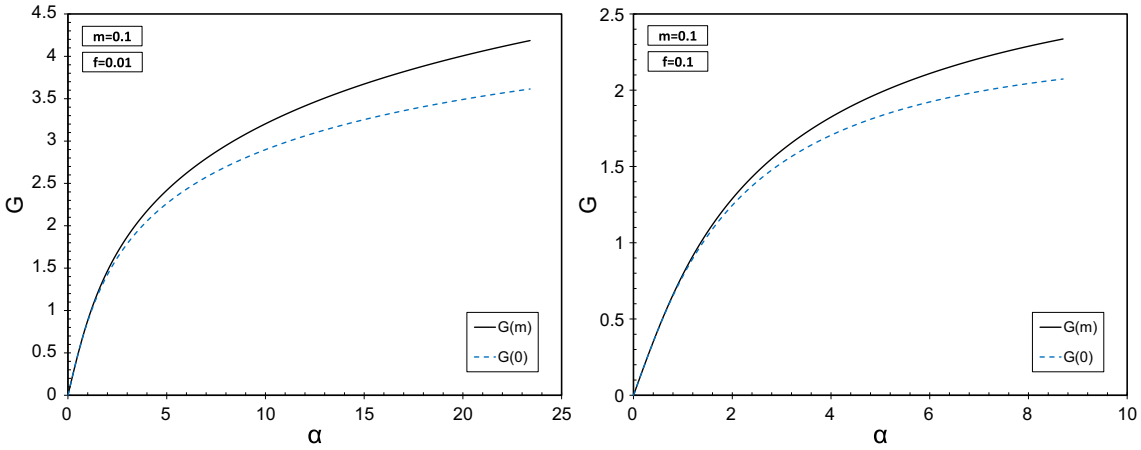

Fig. 3 Variation of $G(m)$ and $G(0)$ versus α for the strain rate sensitivity parameter $m = 0.1$ and the porosity values $f = 0.01$ and $f = 0.1$

series expansion, new analytical approaches to provide accurate macroscopic behavior equations for strain rate power-law materials.

The usefulness of the proposed analytical approximation methods will be explored within the range of triaxialities from 0 (pure torsion) up to $T = 3$. The porosities and strain rate sensitivity parameters are within the intervals $0 \leq f \leq 0.3$, $0 \leq m \leq 0.1$. The proposed ranges are thought to be sufficient to cover the main range of applications of rate sensitive ductile metals. At low-stress triaxiality regime, ductile fracture is controlled by not only void growth, also void shape changes and void rotation under shear-dominated loading are very important. However, since the range of triaxiality considered in this work encompasses low triaxialities, these effects are not taken into account in this work.

3.1 Approximation procedure

We define the functions $G(m)$ and $H(m)$ as:

$$G(m) = \int_{f\cdot\alpha}^{\alpha} (1+x^2)^{\frac{m-1}{2}},$$
$$H(m) = \int_{f\cdot\alpha}^{\alpha} \frac{(1+x^2)^{\frac{m-1}{2}}}{x^2}. \tag{32}$$

The value of m is assumed to be small enough so that we can expand the expression of the integrals $G(m)$ and $H(m)$ into Taylor series at $m = 0$. For simplification, in the present contribution, we only consider the first-order approximation of the series:

$$G(m) = G(0) + m\ G'(0) + R_G,$$
$$H(m) = H(0) + m\ H'(0) + R_H \tag{33}$$

where the truncation errors R_G and R_H in G and H are defined as:

$$R_G = \frac{G''(m_1)}{2!}\, m^2; \quad R_H = \frac{H''(m_2)}{2!}\, m^2; \tag{34}$$

for some m_1 and m_2 between 0 and m. $|R_G| < 0.128$ and $|R_H| < 0.002$.

Let us represent in Figs. 3 and 4, and in order to illustrate the previous assumption, $G(m)$ and $G(0)$ as functions of α, and $H(m)$ and $H(0)$ also as functions of α for $m = 0.1$ and the porosities $f = 0,\ 0.01$ and $f = 0.1$. The values of α in the x-axis cover triaxialities within the interval $0 \leq T \leq 3$ for each m and f value represented. The values of the curves for triaxiality $T = 3$ are marked in the plots with a circle. For other m rate sensitivity parameters and porosities, similar curves are found.

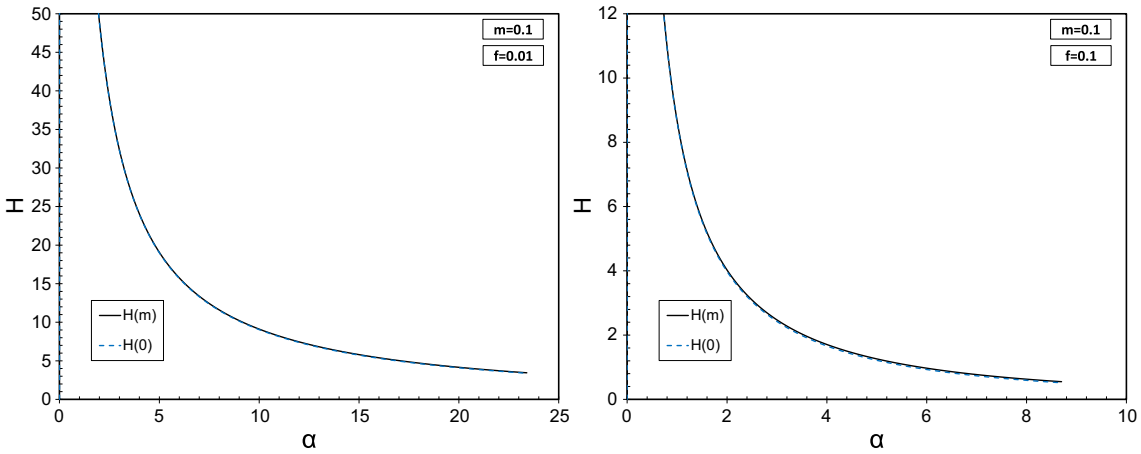

Fig. 4 Evolution of $H(m)$ and $H(0)$ with α for $m = 0.1$ and the porosities $f = 0.01$ and $f = 0.1$

It should be also noted, and as can be verified in Figs. (3) and (4), that:

$$\left|mG'(0) + R_G\right| >>> \left|mH'(0) + R_H\right| \quad \text{with} \quad \left|mH'(0) + R_H\right| < 0.074 \tag{35}$$

holds true for every f, T, and m value analyzed. Under this assumption, the solution of the functions $G(m)$ and $H(m)$ can be further approximated as:

$$\begin{aligned} G(m) &= G(0) + m \cdot G'(0), \\ H(m) &= H(0) \end{aligned} \tag{36}$$

being the functions $G(0)$ and $H(0)$ the f and α-dependent solutions for the case $m = 0$ (classical Gurson yield function) with analytical solution of the form:

$$G(0) = \mathrm{Ln}\left(\frac{\alpha + \sqrt{1+\alpha^2}}{f\cdot\alpha + \sqrt{1+(f\cdot\alpha)^2}}\right); \quad H(0) = \frac{\sqrt{1+f^2\alpha^2} - f\sqrt{1+\alpha^2}}{f\alpha} \tag{37}$$

and $G'(0)$ the integral:

$$G'(0) = \frac{1}{2}\int_{f\cdot\alpha}^{\alpha} (1+x^2)^{-\frac{1}{2}} \ln(1+x^2)\mathrm{d}x, \tag{38}$$

f and α dependent and without analytical solution.

3.2 First closed-form approximation

The following step in the approach is based on the idea that, for the porosities and triaxialities analyzed, the relation $\left(1 - \frac{f\alpha}{\sqrt{3}}\right)$ can be approximated to 1 that allows, from Eq. (31), to propose the identity ($\dot{E}_3 = \dot{E}_{\mathrm{eq}}$). Considering also the assumption made in Eq. (36), the relations given in Eqs. (29), (30) can be now written in the form:

$$\frac{\Sigma_1}{\sigma_0 \cdot \dot{E}^m_{\mathrm{eq}}} = \frac{\sqrt{3}}{3}\left(G(0) + m \cdot G'(0)\right), \tag{39}$$

$$\frac{\Sigma_{\mathrm{eq}}}{\sigma_0 \cdot \dot{E}^m_{\mathrm{eq}}} = f \cdot \alpha \cdot H(0). \tag{40}$$

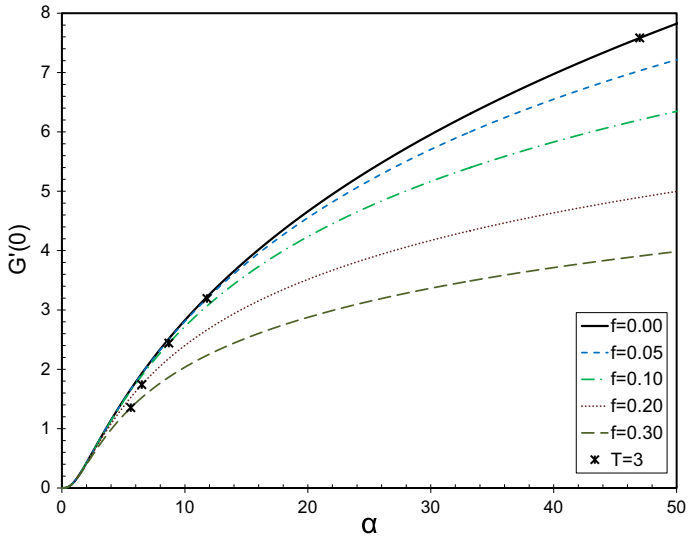

Fig. 5 Evolution of $G'(0)$ versus the parameter α for $f = 0,\ 0.05,\ 0.1,\ 0.2$ and 0.3

Defining the dimensionless stress variables:

$$\widehat{\Sigma}_1 = \frac{\Sigma_1}{\sigma_0 \cdot \dot{E}_{\text{eq}}^m}; \quad \widehat{\Sigma}_{\text{eq}} = \frac{\Sigma_{\text{eq}}}{\sigma_0 \cdot \dot{E}_{\text{eq}}^m} \tag{41}$$

and following the same procedure as in the previous Section for rate-independent materials, for a porous plastic rate-dependent material, the first proposed closed-form $\widehat{\Sigma}_1 - \widehat{\Sigma}_{\text{eq}}$ relation can now be written as:

$$\Phi\left(\widehat{\Sigma}_{\text{eq}}, \widehat{\Sigma}_1, f, G'(0), m\right) = \left(\widehat{\Sigma}_{\text{eq}}\right)^2 + 2f\cosh\left(\sqrt{3}\widehat{\Sigma}_1 - mG'(0)\right) - (1+f^2) = 0. \tag{42}$$

From this point on, the goal is that of approximating $G'(0)$ Eq. (38) via a simple and accurate function that allows the function Φ given in Eq. (42) to be defined in terms of the variables f, m, $\widehat{\Sigma}_1$, and $\widehat{\Sigma}_{\text{eq}}$.

Figure 5 represents the evolution of $G'(0)$ with α for different values of porosity ($f = 0, 0.05, 0.1, 0.2$, and 0.3). In addition, for each porosity, $G'(0)$ as function of α is marked by an asterisk (*) for triaxiality $T = 3$. For the range of f values analyzed ($0 \leq f \leq 0.3$), it can be easily proved that the differences in $G'(0)$ between the reference case ($f = 0$) and the rest of porosities studied do not exceed, for ($0 \leq T \leq 3$), 18.7%. For the sake of simplicity, let us adopt a logarithmic fitting function, only α dependent, to approximate the integral $G'(0)$:

$$G'_{0\,\text{Fitted}} = A_1 \cdot \text{Log}_{10}\left(\frac{\alpha}{A_2} + 1\right). \tag{43}$$

A_1 and A_2 are defined as two fitting parameters of the proposed approximated function to $G'(0)$ for the case with $f = 0$ in ($0 \leq T \leq 3$). The values of the fitting parameters, obtained using a least squares method, are $A_1 = 10.56$ and $A_2 = 11.50$ (see Fig. 6).

As shown in Fig. 7a, b, $f\alpha H(0) = \widehat{\Sigma}_{\text{eq}}$ is well approximated, for different values of f ($f = 0.01,\ f = 0.1$ in the Figures), by the linear function:

$$\widehat{\Sigma}_{\text{eq}} = (1-f) - B(f) \cdot \alpha \tag{44}$$

that allows α to be written as function of $\widehat{\Sigma}_{\text{eq}}$ and f without loss of significant accuracy:

$$\alpha_{\text{Fitted}} = \frac{1 - f - \widehat{\Sigma}_{\text{eq}}}{B(f)}. \tag{45}$$

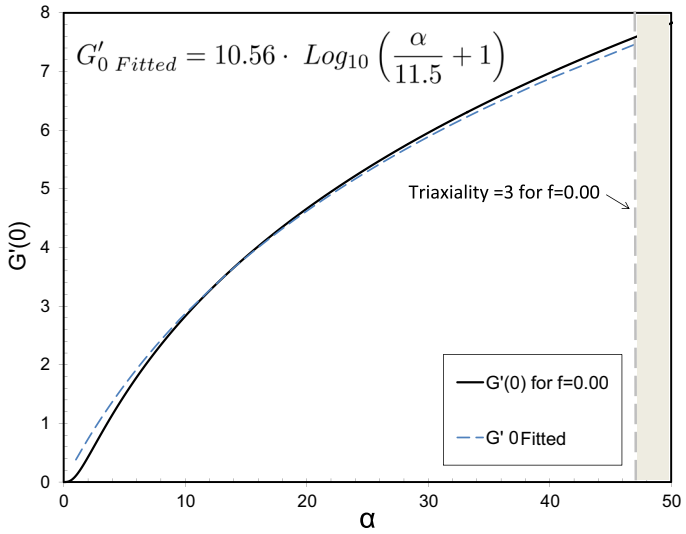

Fig. 6 Comparison of $G'(0)$ for $f = 0$ and $G'_{0\ Fitted}$ versus α

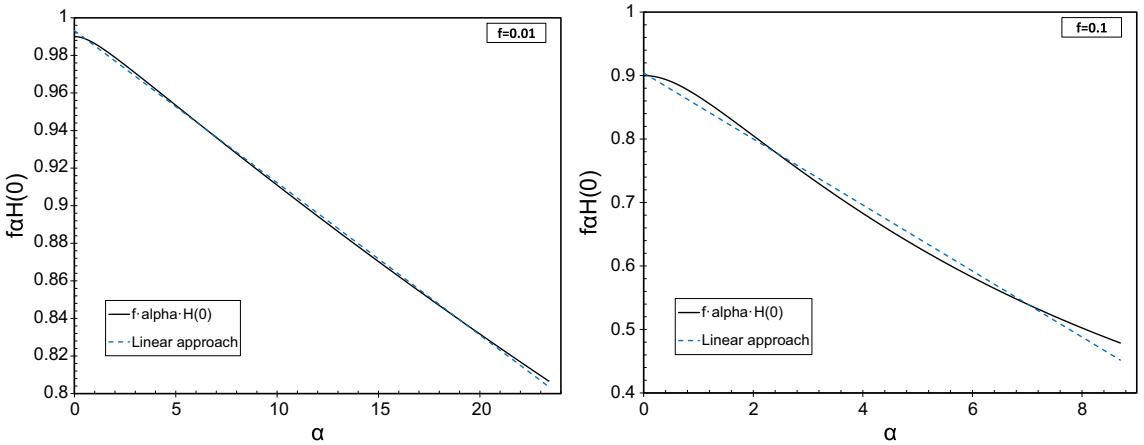

Fig. 7 Comparison between the $f\alpha H(0) - \alpha$ curve and the fitting linear approaches (using a least squares, method) for $f = 0.01$ and $B = 0.008$ (**a**), and $f = 0.1$ and $B = 0.052$ (**b**)

Table 1 B fitting values

f	0	0.001	0.01	0.025	0.05	0.075	0.1	0.2	0.3
B	0.000	0.001	0.008	0.019	0.032	0.046	0.052	0.079	0.087

To obtain $B(f)$, several porosities in the range $0 \leq f \leq 0.3$ have been checked. The optimal B values for $f = 0, 0.001, 0.01, 0.025, 0.05, 0.075, 0.1, 0.2$, and 0.3 are the ones given in Table 1 (obtained using a least squares fitting method for the range of triaxialities $0 \leq T \leq 3$).

In an attempt to define the continuous field $B(f)$ from Eq. (44), let us propose the polynomial function:

$$B(f) = B_1 \cdot f + B_2 \cdot f^2 \tag{46}$$

that can be calibrated from the discrete B values given in Table 1 (Fig. 8). The interpolation coefficients that are obtained are $B_1 = 0.63$ and $B_2 = -1.17$.

To summarize what is mentioned above, the first proposed closed-form macroscopic function to describe the behavior of strain-dependent materials can be written as:

$$\Phi\left(\widehat{\Sigma}_{\text{eq}}, \widehat{\Sigma}_1, f, m\right) = \left(\widehat{\Sigma}_{\text{eq}}\right)^2 + 2f\cosh\left(\sqrt{3}\widehat{\Sigma}_1 - mG'_{0\ \text{Fitted}}\right) - (1 + f^2) = 0 \tag{47}$$

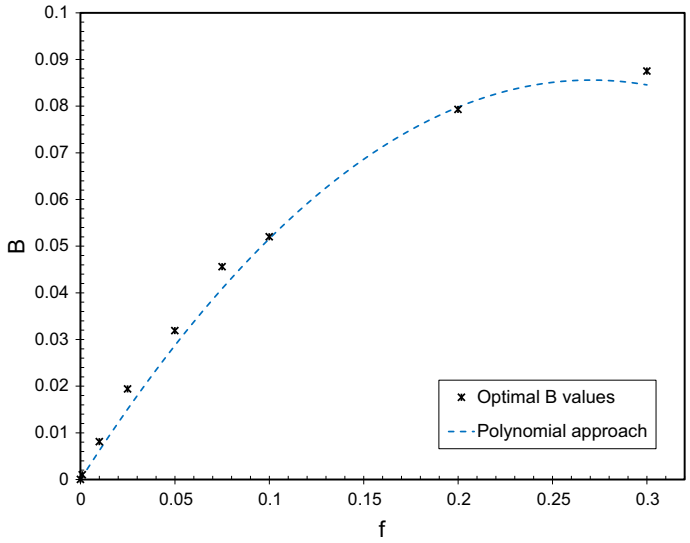

Fig. 8 Polynomial quadratic interpolation function for $B(f)$

with

$$G'_{0\,\mathrm{Fitted}} = A_1 \cdot \mathrm{Log}_{10}\left(\frac{\alpha_{\mathrm{Fitted}}}{A_2} + 1\right); \qquad \alpha_{\mathrm{Fitted}} = \frac{1 - f - \widehat{\Sigma}_{\mathrm{eq}}}{B_1 f + B_2 f^2} \tag{48}$$

and the four parameters:

$$A_1 = 10.56; \quad A_2 = 11.50; \quad B_1 = 0.63; \quad B_2 = -1.17. \tag{49}$$

It should be noted here that the parameters of the proposed model are all material independent.

3.3 Second closed-form approximation

As a second step, and in order to improve the description of the Gurson yield model, we shall not consider the assumption $1 - \frac{f\alpha}{\sqrt{3}} \approx 1$ made in the first approximation of the macroscopic function Φ. The approximation will be improved taking into account the relation given in Eq. (48):

$$1 - \frac{f\alpha}{\sqrt{3}} = 1 - \frac{1 - f - \widehat{\Sigma}_{\mathrm{eq}}}{\sqrt{3}\,(B_1 + B_2 f)}. \tag{50}$$

From Eq. (31):

$$\dot{E}_3 = \frac{\dot{E}_{\mathrm{eq}}}{\left(1 - \frac{1-f-\widehat{\Sigma}_{\mathrm{eq}}}{\sqrt{3}(B_1 + B_2 f)}\right)}. \tag{51}$$

. or simplifying:

$$\dot{E}_3 = \frac{\dot{E}_{\mathrm{eq}}}{K_F}. \tag{52}$$

being K_F the factor:

$$K_F = \left(1 - \frac{1 - f - \widehat{\Sigma}_{\mathrm{eq}}}{\sqrt{3}\,(B_1 + B_2 f)}\right); \tag{53}$$

$B_1 = 0.63$, $B_2 = -1.17$.

The proposed relations provide a new expression for the Gurson-type function Φ for strain-rate-dependent materials given in the form:

$$\Phi\left(\widehat{\Sigma}_{\text{eq}},\,\widehat{\Sigma}_1,\,f,\,G'(0),\,m\right)=\left((K_F)^m\,\widehat{\Sigma}_{\text{eq}}\right)^2+2f\cosh\left(\sqrt{3}((K_F)^m\cdot\widehat{\Sigma}_1)-mG'(0)\right)-(1+f^2)=0 \tag{54}$$

with

$$G'(0)=A_1\cdot\text{Log}_{10}\left(\frac{1-f-\widehat{\Sigma}_{\text{eq}}}{A_2\left(B_1f+B_2f^2\right)}+1\right),\quad K_F=\left(1-\frac{1-f-\widehat{\Sigma}_{\text{eq}}}{\sqrt{3}\left(B_1+B_2f\right)}\right) \tag{55}$$

and the four material-independent parameters of the model given in Eq. (49):

$$A_1=10.56;\ A_2=11.50;\ B_1=0.63;\ B_2=-1.17. \tag{56}$$

4 Validation of the proposed macroscopic functions

We will further assess the accuracy of the two criteria proposed. First, and with the aim to validate the approximations made in the analytic evaluation of the macroscopic surfaces, we will present comparisons between the proposed closed relations for macroscopic $\hat{\Sigma}_1-\hat{\Sigma}_{\text{eq}}$ stresses and the "*exact*" solution obtained by numerically integrating Eqs. (29) and (30). Second, and in order to assess the approximations of Eq. (47) and (54), we will also present comparisons between the derived approximate relations and the results obtained by numerical calculations using a commercial finite element code. Numerical finite element calculations are made considering the yield locus originally proposed by Gurson and taking into account the strain rate dependence replacing σ_0 by the yield stress $\bar{\sigma}$ of the matrix material.

4.1 Cell model and numerical implementation

Theoretical results will be validated performing unit cell analysis. This versatile numerical methodology was first introduced by Koplik and Needleman [24] and Brocks et al. [25], and allows to easily study the effect of various micromechanical ductile parameters such as second phase particles and void population [26–29], void shape or cell shape [8], material anisotropy [30], the effects of complex stress states [31–34] or matrix hardening rate behavior [35–37].

Numerical simulations were carried out using the commercial finite element code ABAQUS/Standard [38]. The representative elementary cell volume is a cylindrical cell having an initial half length H_0 and a radius $R_0=H_0/2$. Due to the symmetry of the problem with respect to $Z=0$, only the $Z\geq 0$ half of the cell is analyzed. The cell is homogeneous, and the evolution of the void volume fraction f is governed by the void evolution law from the Gurson model. (There is no explicit void located in the cell.) The 2D, axisymmetric mesh used in the computations is represented in Fig. 9 in its undeformed configuration. The mesh is made of 50 axisymmetric quadrilateral 8-node elements with reduced integration (CAX8R).

The boundary conditions on the outer surfaces of the homogeneous cell are specified as:

$$\begin{aligned} u_1&=U_1,\quad \text{for}\quad X_1=R; &\qquad u_1&=0,\quad \text{for}\quad X_1=0,\\ u_3&=U_3,\quad \text{for}\quad X_3=H; &\qquad u_3&=0.\quad \text{for}\quad X_3=0. \end{aligned}$$

U_1 and U_3 are calculated such that the macroscopic transverse stress Σ_1 in the cylindrical surface:

$$\Sigma_1=\frac{1}{H}\int_0^H[\sigma_1]_{X_1=R}\,\text{d}X_3, \tag{57}$$

and the macroscopic axial stress Σ_3 in the top surface:

$$\Sigma_3=\frac{2}{R^2}\int_0^R[\sigma_3]_{X_3=H}\;X_1\cdot\text{d}X_1 \tag{58}$$

as prescribed values during the whole loading history. σ_1 and σ_3 are the Cauchy stress components, and $R=R_0+U_1$, $H=H_0+U_3$. This strategy, used by different authors [35,39,40] to prescribe boundary conditions, allows to overcome numerical problems associated with cell softening due to void growth. For

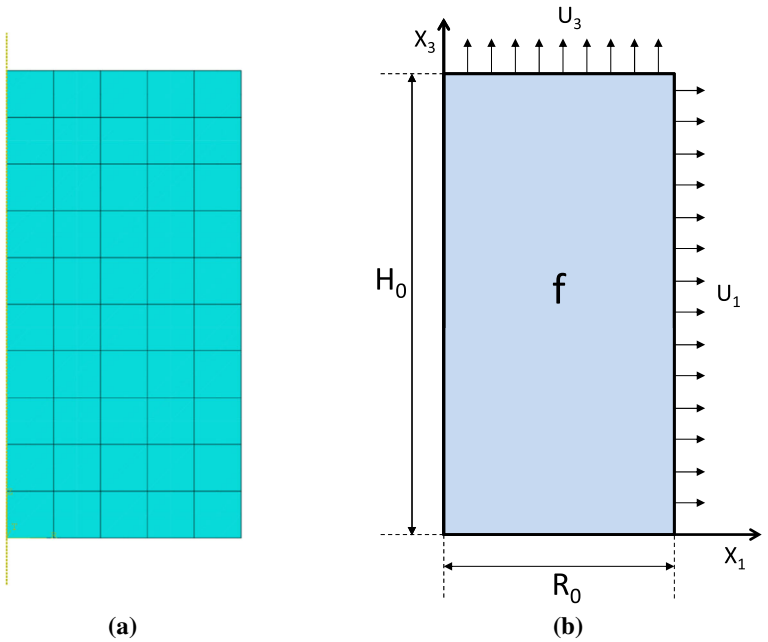

Fig. 9 Initial mesh of the cylinder (**a**) and displacement boundary conditions imposed on the unitary cell (**b**)

further details of this procedure see Vadillo and Fernández-Sáez [40]. Displacement boundary conditions are implemented in a finite element code [38] via an MPC routine.

For hypoelastic-plastic materials, the macroscopic rate of plastic deformation tensor, $\dot{\mathbf{E}}^p$, is related with the macroscopic stress rate by:

$$\dot{\mathbf{\Sigma}} = \mathbf{C} : \left(\dot{\mathbf{E}} - \dot{\mathbf{E}}^p\right) \tag{59}$$

with $\mathbf{C}$ the tensor of isotropic elastic moduli:

$$\mathbf{C} = 2G\mathbf{I}' + K\mathbf{1} \otimes \mathbf{1} \tag{60}$$

and $G = E/(2(1+\nu))$ and $K = E/(3(1-2\nu))$ elastic constants. E is Young's modulus, and ν is Poisson's ratio. $\mathbf{I}'$ is the unit deviatoric fourth-order tensor with the form:

$$(\mathbf{I}')_{ijkl} = \frac{1}{2}(\delta_{ik}\delta_{jl} + \delta_{il}\delta_{jk}) - \frac{1}{3}\delta_{ij}\delta_{kl}. \tag{61}$$

The ductile material is approximated using Gurson [3]'s criterion for cylindrical voids, with the yield condition of the form:

$$\Phi = \frac{\Sigma_{\text{eq}}^2}{\bar{\sigma}^2} + 2\, f \cosh\left(\frac{\sqrt{3}\ \Sigma_1}{\bar{\sigma}}\right) - (1 + f^2) = 0 \tag{62}$$

where the Mises stress $\bar{\sigma}$ is described by the power-law equation:

$$\bar{\sigma} = \sigma_Y \left(\frac{\dot{\varepsilon}}{\dot{\varepsilon}_0}\right)^m. \tag{63}$$

The evolution of void volume fraction, considering only growth, can be written as:

$$\dot{f} = (1 - f)\dot{\mathbf{E}}^p : \mathbf{1} \tag{64}$$

with $\dot{\mathbf{E}}^p$:

$$\dot{\mathbf{E}}^p = \dot{\lambda}\frac{\partial \Phi}{\partial \mathbf{\Sigma}}, \tag{65}$$

and the plastic proportionality factor $\dot{\lambda}$:

$$\dot{\lambda} = \frac{(1-f)\bar{\sigma}\dot{\bar{\varepsilon}}^p}{\boldsymbol{\Sigma} : \frac{\partial \Phi}{\partial \boldsymbol{\Sigma}}}, \tag{66}$$

To complete the above formulation, the Kuhn–Tucker loading–unloading conditions should be considered. This implies that $\dot{\lambda} = 0$ and $\Phi < 0$ during elastic loading or unloading, and $\dot{\lambda} > 0$ and $\Phi = 0$ during plastic yielding.

The values of the reference material parameters are taken to be $E = 200\,\text{GPa}$, $\nu = 0.3$, $\sigma_Y = 2000$ MPa, $\dot{\varepsilon}_0 = 1\ \text{s}^{-1}$, and $m = 0.01,\ 0.05$, and 0.1. These values of strain rate sensitivity parameter are used to model a wide variety of metallic materials, e.g., Gosh [41], Klöcker and Tvergaard [42]

The set of constitutive nonlinear equations is integrated into a finite element scheme at the level of a material point. Two different tasks should be carried out. The first one is related to update stress and state variables driven by the strain increment. The second one consists in creating a consistent tangent operator to preserve the quadratic convergence in the iterative solution based on Newton's method. The algorithm is implemented in the commercial Finite Element code ABAQUS/Standard [38] by a UMAT user subroutine. Details of the implementation can be found in [40,43].

4.2 Comparison between the exact solution and the proposed macroscopic functions

First approximation

Results of the macroscopic behavior of a porous rate-dependent material, according to the first approximation given in Eq. (47), are presented in Fig. 10 for $f = 0.01$, $f = 0.05$, and $f = 0.1$ in the $\widehat{\Sigma}_1 - \widehat{\Sigma}_{\text{eq}}$ space considering $m = 0.01$ (a), $m = 0.05$ (c), and $m = 0.1$ (d). These results are compared with the *"exact"* solution obtained by numerically integrating Eqs. (29) and (30). The range of triaxiality values analyzed comes from $T = 0$ up to $T = 3$. As shown in Fig. 10a for $m = 0.01$, both macroscopic surfaces practically coincide for all the porosities studied in the whole stress range. However, for higher m values, the differences between both functions increase as f values increase (see Fig. 10c, e), being in all the cases the approximated curve for $\hat{\Sigma}_1 - \hat{\Sigma}_{\text{eq}}$ below that corresponding to the "exact" representation. Note that for every f value the new proposed $\hat{\Sigma}_1 - \hat{\Sigma}_{\text{eq}}$ relations reduce to the existing Gurson yield locus if $m = 0$.

Second approximation

Figure 10b, d, and f show that the closed-form macroscopic function proposed in Eq. (54) practically coincides with the exact solution for $m = 0.01$ and slightly under-predicts the exact solution for $m = 0.05$ and $m = 0.1$. The surface obtained considering the second approximation procedure thus satisfactorily reproduces the rate-dependent material behavior for all the porosities analyzed over the range ($0 \leq f \leq 0.3$) in triaxialities ($0 \leq T \leq 3$) retrieving again the classical Gurson formulation for null strain rate ($m = 0$).

4.3 Comparison between the classical Gurson yield locus and the new behavior equations

The classical Gurson model is a rate-independent plasticity model. For rate-dependent materials, the Gurson-type yield surface is usually not modified, and rate dependence is taken into account replacing σ_0 by the yield stress of the matrix material $\bar{\sigma}$. The matrix stress rate dependence indirectly introduces a rate dependence to the Gurson flow potential. However, this simple assumption has little physical meaning and could not be always valid. In the following Section, numerical simulations using the classical Gurson model are developed using a finite element code, and results are compared with the exact solution of the macroscopic behavior of the material in the $\hat{\Sigma}_1 - \hat{\Sigma}_{\text{eq}}$ space. Also and in order to assess the accuracy and usefulness of the proposed macroscopic surfaces, the numerical finite element results are compared with the ones obtained with the suggested approximate closed-form expressions.

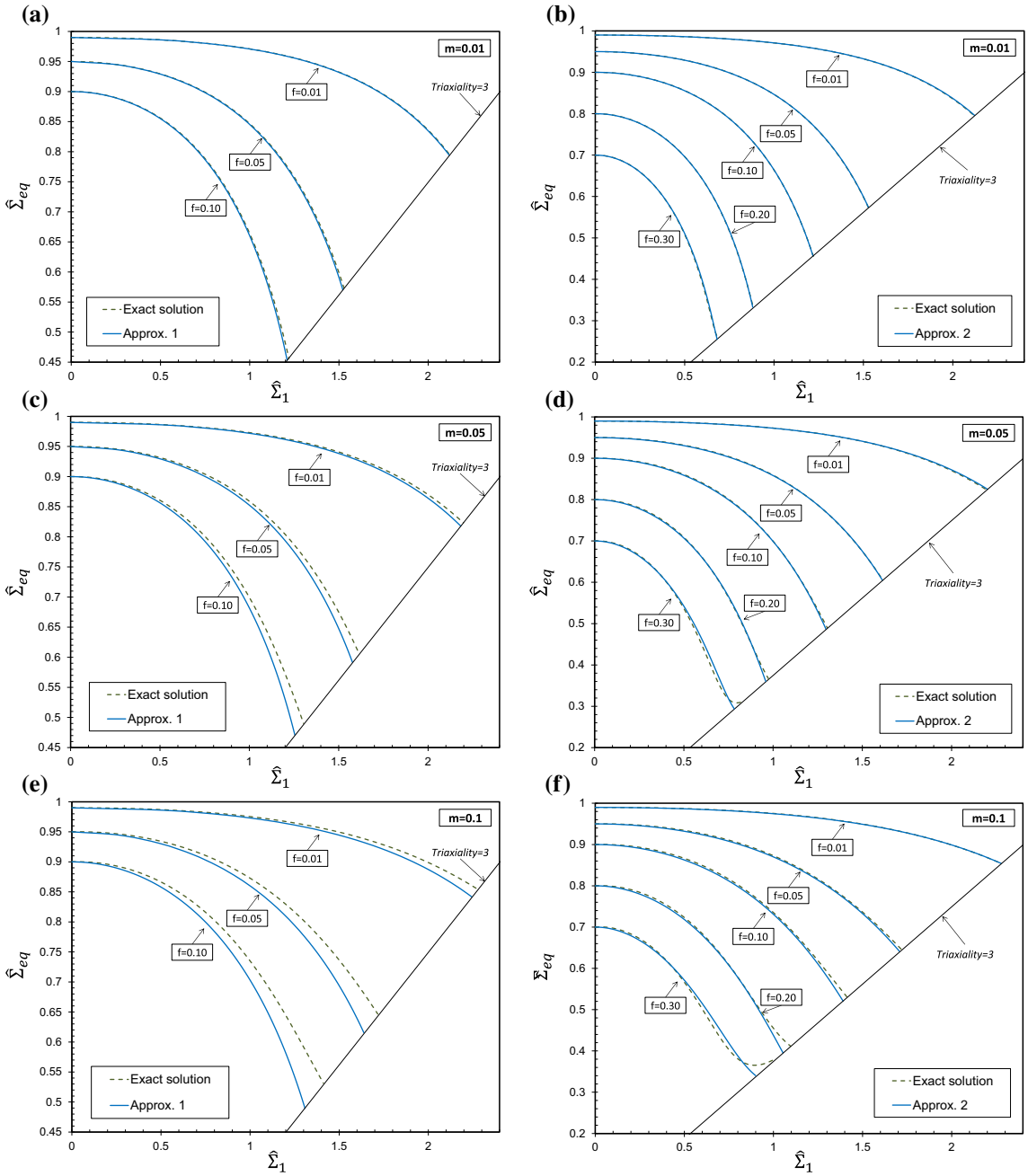

Fig. 10 Comparison of model and exact $\widehat{\Sigma}_{\text{eq}} - \widehat{\Sigma}_1$ relation considering the first approach (**a**, **c**, **e**) and the second criterion (**b**, **d**, **f**) for $f = 0.01, 0.05, 0.1$ (**a**, **c**, **e**), for $f = 0.01, 0.05, 0.1, 0.2, 0.3$ (**b**, **d**, **f**), and for $m = 0.01$ (**a**, **b**), $m = 0.05$ (**c**, **d**), and $m = 0.1$ (**e**, **f**)

First approximation

Numerical simulations using the finite element code [38] are presented for a rate-dependent power-law material considering different values of strain rate sensitivity parameter m, and various values of porosities f and triaxialities T. The obtained macroscopic relations are compared with the ones calculated with the exact solution and with the first-approximated closed-form analytic expression given in Eq. (42).

In Fig. 11a, c, and e, we represent the macroscopic $\hat{\Sigma}_1 - \hat{\Sigma}_{\text{eq}}$ relations for the porosity values $f = 0.01$, $f = 0.05$, and $f = 0.1$, respectively, for the strain rate sensitivity parameters $m = 0.01$, 0.05, and $m = 0.1$, and for the range of triaxialities $0 \leq T \leq 3$. The full and broken lines correspond to the exact and

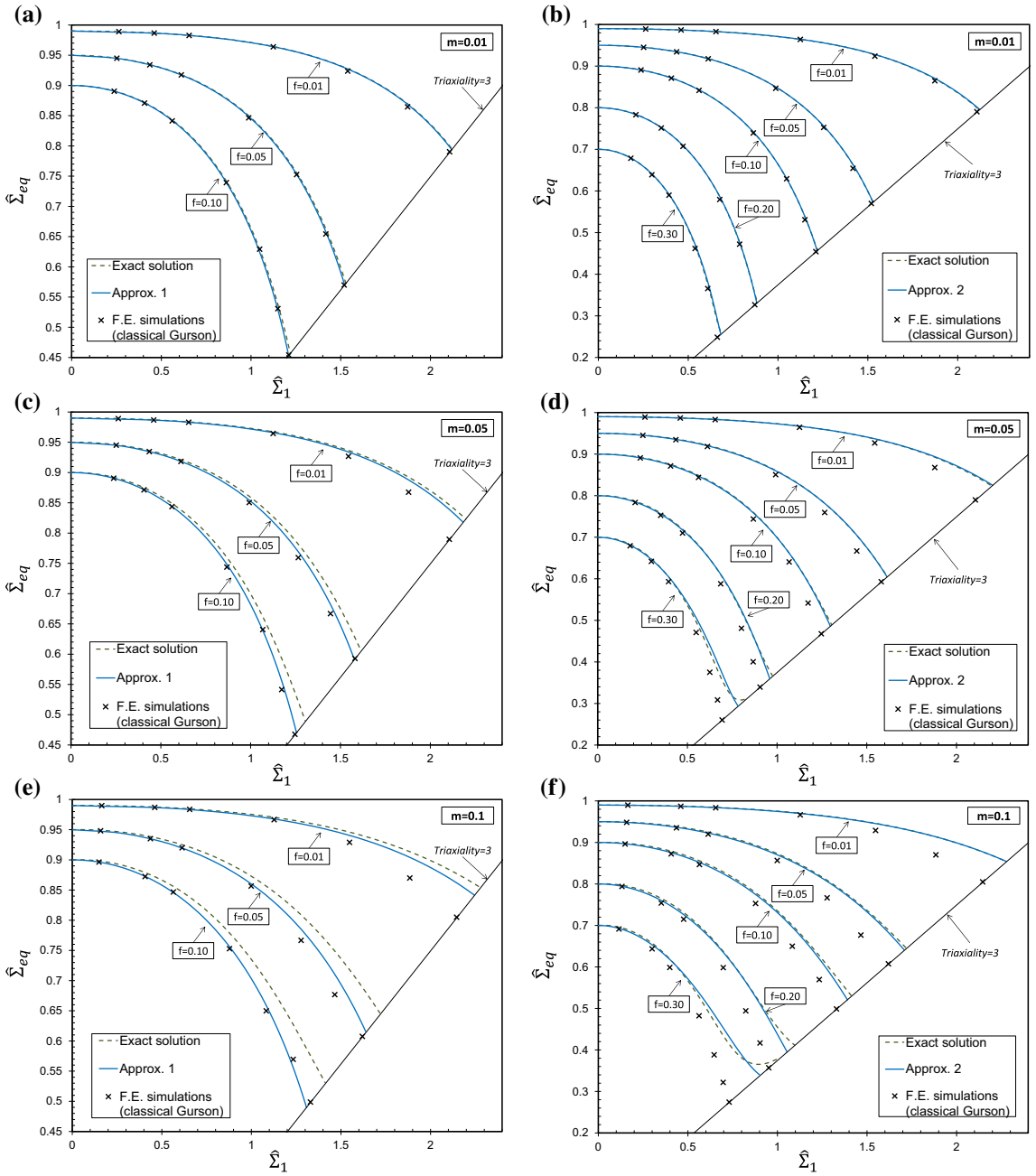

Fig. 11 Comparison of model, numerical finite element, and exact $\widehat{\Sigma}_{\text{eq}} - \widehat{\Sigma}_1$ results considering the first approximation (**a**, **c**, **e**) and the second proposed approximate macroscopic surfaces (**b**, **d**, **f**), for $f = 0.01, 0.05, 0.1$ (**a**, **c**, **e**), for $f = 0.01, 0.05, 0.1, 0.2, 0.3$ (**b**, **d**, **f**), and for $m = 0.01$ (**a**, **b**) , $m = 0.05$ (**c**, **d**), and $m = 0.1$ (**e**, **f**)

approximated closed-form solutions of the problem. The asterisks (*) correspond to the values obtained by the finite element numerical computations. A good agreement between the exact, approximate, and numerical criteria is observed for all the analyzed porosities if $m = 0.01$. It must be emphasized that for $m = 0.05$ and $m = 0.1$ the numerical finite element results differ from the exact solution for all porosities when increasing the variable $\widehat{\Sigma}_1$ (or when increasing the triaxiality T values). For the highest values of f, the analytical first-approximated solution exhibits the same accuracy as the one obtained with the finite elements. For the smaller f values, the accuracy of the analytical solution is better. The improvement in the results if the value of f is

small is attributed to the approaches taken in the analytical solution (closer to the exact solution as far as f is closer to 0).

Second approximation

Figure 11b, d, and f compare the exact solution, the second analytical approach, and the finite element simulations of the $\hat{\Sigma}_1 - \hat{\Sigma}_{eq}$ surface for different porosities and strain rate sensitivity parameters. As shown in Fig. 11b, for $m = 0.01$, all solutions converge to a single continuous curve. For higher values of m, the given second analytical approach is in closer agreement with the exact solution if the results are compared with numerical simulations obtained taking into account the effect of strain rate by replacing σ_0 by $\bar{\sigma}$ in the classical Gurson yield function.

4.4 Comparison with other viscoplastic models

The aim of the present Section is to compare the predictions of the proposed second analytical formulation with other models previously developed and validated. In particular, the porous metal Leblond–Perrin–Suquet's [22] (LPS) theory is used in order to check the predictive power of this work when it is compared with that one. Following [22], the LPS formulation for power-law viscoplastic voided cylindrical solids is given by the relations:

$$\bar{\Psi}_a(Q, M) = Q^2 + f\left(h(M) + \frac{1-m}{1+m}\frac{1}{h(M)}\right) - 1 - \frac{1-m}{1+m}f^2,$$
$$h(M) = \left(1 + m\left(\sqrt{3}|M|\right)^{m+1}\right)^{1/m}, \tag{67}$$

with Q and M defined in terms of the gauge factor Λ as $Q = \Sigma_{eq}/\Lambda$ and $M = (\Sigma_1 + \Sigma_2)/(2\Lambda)$ with $\Sigma_1 = \Sigma_2$. The upper bound for the approximate macroscopic potential, Ψ_m, is given by [22]:

$$\Psi_m(\boldsymbol{\Sigma}, f) = \frac{\sigma_Y \dot{\varepsilon}_0\, m}{m+1}\left(\frac{\Lambda(\boldsymbol{\Sigma}, f)}{\sigma_Y}\right)^{\frac{m+1}{m}} = \frac{\sigma_Y \dot{\varepsilon}_0\, m}{m+1}(1-f), \tag{68}$$

and the strain rates $\dot{E}_1$, $\dot{E}_2$, and $\dot{E}_3$ can be calculated from Ψ_m using the relations [22]:

$$\dot{E}_1 = \frac{\partial \Psi_m}{\partial \Sigma_1}, \quad \dot{E}_2 = \frac{\partial \Psi_m}{\partial \Sigma_2}, \quad \dot{E}_3 = \frac{\partial \Psi_m}{\partial \Sigma_3}. \tag{69}$$

In the LPS model, for the cylindrical case and for a given ratio $\rho = \Sigma_{eq}/\Sigma_1$, one can determine the point (M, Q) of the gauge surface corresponding to any strain rate parameter m, porosity f, and ratio M by computing Eq. (67) with $\bar{\Psi}_a(M, \rho M) = 0$. Once the value of M is calculated, and being the gauge factor's value $\Lambda = \Sigma_1/M$, the point with coordinates $(\Sigma_1, \rho\Sigma_1)$ of the Leblond–Perrin–Suquet upper bound macroscopic potential Ψ_m can be derived from given f, m, ρ, and M values using Eq. (68) for any σ_Y and $\dot{\varepsilon}_0$. The corresponding macroscopic strain rate relations $\dot{E}_1$ and $\dot{E}_3$ follow by differentiation of the potential Ψ_m with respect to $\boldsymbol{\Sigma}$. In the Leblond–Perrin–Suquet upper bound potential, a point $\Psi_m(\Sigma_1, \rho\Sigma_1)$ lies on the $\widehat{\Sigma}_1 - \widehat{\Sigma}_{eq}$ space with $\widehat{\Sigma}_1 = \Sigma_1/\left(\sigma_Y\left(\dot{E}_{eq}/\dot{\varepsilon}_0\right)^m\right)$, $\widehat{\Sigma}_{eq} = \rho\,\widehat{\Sigma}_1$, and $\dot{E}_{eq} = \frac{2}{3}\left(\dot{E}_3 - \dot{E}_1\right)$ from Eq. (69). Thus, for given σ_Y, $\dot{\varepsilon}_0$, ρ, f and m values, the relation $(\widehat{\Sigma}_1 - \widehat{\Sigma}_{eq})$ in the LPS model requires the solution of all the variables Λ, Σ_1, $\dot{E}_1$, and $\dot{E}_3$ that entail, according to the authors' opinion, in non-negligible computing costs.

Figure 12 shows plots for $(\widehat{\Sigma}_1 - \widehat{\Sigma}_{eq})$ relations for the porosities ($f = 0.01,\ 0.05, 0.1, 0.2, 0.3$) and (a) $m = 0.01$ and (b) $m = 0.1$. The second approach proposed in this work is compared with the exact solution and LPS predictions. In these plots, it is observed that the proposed analytical approach is in good agreement with the LPS model and the exact solution for the whole range of stress triaxialities and porosities analyzed. In practice, however, the approach suggested is a simpler alternative to the problem at hand.

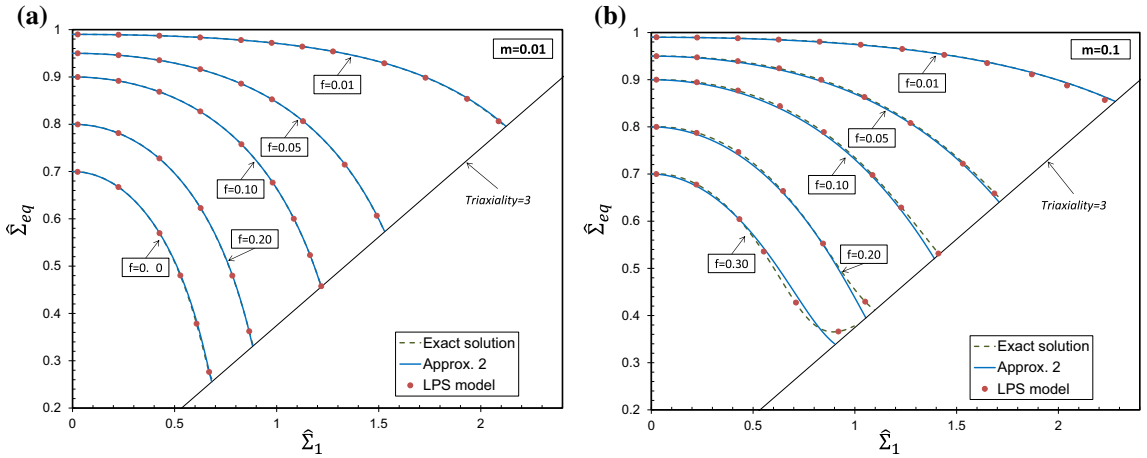

Fig. 12 Macroscopic surfaces according to the proposed criterion (Eq. (54)), in comparison with the LPS model [22] and exact solution for the porosities ($f = 0.01,\ 0.05,\ 0.1,\ 0.2,\ 0.3$) and strain rate parameters $m = 0.01$ (**a**), and $m = 0.1$ (**b**)

5 Conclusions and remarks

Reliable characterization of viscoplastic ductile materials and precise modeling of ductile damage processes are of significant importance for a better understanding of engineering applications like cutting, machining or metal forming. In this paper, a modification of the Gurson criterion for cylindrical voids is extended by incorporating the strain rate dependence of the matrix material. Analytical closed-form approximate expressions of the macroscopic behavior of viscoplastic power-law porous materials have been obtained and assessed by its comparison with the "*exact*" solutions obtained by computing numerically the integrals in Eqs. (29), (30). The derivation of the macroscopic functions is based on a Taylor series expansion at strain rate parameter $m = 0$. Certain additional approximations are introduced in order to obtain analytical closed-form expressions. Two accurate explicit macroscopic functions are constructed: (a) The first one is analytically simpler. The derived first criterion exhibits very good results for strain rate sensitivity parameters $m \leq 0.05$ for the range of porosities and triaxialities tested ($f \leq 0.1,\ 0 \leq T \leq 3$). (b) The second approach is a bit more complex than the first one. Nevertheless, for this second approximation, the ability to accurately describe the behavior of viscoplastic materials is very good also for the high strain rate parameters tested ($m = 0.1$) for an extended range of porosities ($0 \leq f \leq 0.3$). For $m = 0$, both approaches reduce to Gurson's model. It is important to note that, for the proposed homogenized Gurson-type behavior equations, the required parameters of the models are all material independent.

Furthermore, we also compare the exact solution and the analytical approximated closed-form macroscopic surfaces with numerical simulations performed using a finite element code (ABAQUS/Standard). In the numerical finite element simulations, the strain rate dependence of ductile materials is characterized replacing, in the original Gurson yield locus, the constant flow stress term σ_0 by a rate-dependent flow stress term $\bar{\sigma} = \sigma_0\left(\dot{\bar{\varepsilon}}\right)$. The results presented above evidence a progressive loss of accuracy of the classical model of [3] as the strain rate parameter m increases. The loss of accuracy is important for rate sensitivity parameters $m \geq 0.05$.

For the large range of porosities and triaxialities analyzed, the key findings of this study are summarized as follows:

- For small m strain rate sensitivity parameters ($m < 0.05$), all macroscopic surfaces presented have practically the same behavior.
- For high m parameters ($m \geq 0.05$), both analytical closed-form functions (first and second approach) have the important quality to better predict the behavior of rate sensitive materials than the classical Gurson model.
- The improved accuracy of the second approach allows to model the behavior of rate sensitive power-law ductile materials for porosities up to 0.3.

The proposed second approach also has shown, when compared with other viscoplastic models, to be accurate and simpler as others. The proposed formulation is then suitable for power-law rate sensitive materials and can be easily implemented into finite element codes.

Acknowledgements The authors would like to thank Professor Sébastien Mercier, from Université de Lorraine, for valuable discussions. The authors are indebted to the Spanish Ministry of Economy and Competitiveness (Projects EUIN2015-62556 and DPI2014-57989-P) for the financial support received which allowed conducting part of this work. The research leading to these results has received funding from the European Union's Horizon2020 Programme (Excellent Science, Marie-Sklodowska-Curie Actions) under REA Grant Agreement 675602 (Project OUTCOME).

References

1. McClintock, F.A.: A criterion for ductile fracture by the growth of holes. J. Appl. Mech. **35**, 363 (1968)
2. Rice, J.R., Tracey, D.M.: On the ductile enlargement of voids in triaxial stress fields. J. Mech. Phys. Solids **17**, 201 (1969)
3. Gurson, A.: Continuum theory of ductile rupture by void nucleation and growth: part I—yield criteria and flow rules for porous ductile media. J. Eng. Mater. Technol. **99**, 2 (1977)
4. Chu, C., Needleman, A.: Void nucleation effects in biaxially stretched sheets. J. Eng. Mater. Technol. **102**, 249 (1980)
5. Tvergaard, V., Needleman, A.: Analysis of cup-cone fracture in a round tensile bar. Acta Metall. **32**, 157 (1984)
6. Gologanu, M., Leblond, J., Devaux, J.: Approximate models for ductile metals containing nonspherical voids-case of axisymmetric prolate ellipsoidal cavities. J. Mech. Phys. Solids **41**, 1723 (1993)
7. Gologanu, M., Leblond, J., Devaux, J.: Approximate models for ductile metals containing nonspherical voids-case of axisymmetric oblate ellipsoidal cavities. J. Eng. Mater. Technol. **116**, 290 (1994)
8. Pardoen, T., Hutchinson, J.: An extended model for void growth and coalescence. J. Mech. Phys. Solids **48**, 2467 (2000)
9. Madou, K., Leblond, J.: A Gurson-type criterion for porous ductile solids containing arbitrary ellipsoidal voids I: limit-analysis of some representative cell. J. Mech. Phys. Solids **60**, 1020 (2012)
10. Leblond, J.B., Perrin, G., Devaux, J.: An improved Gurson-type model for hardenable ductile metals. Eur. J. Mech. A Solids **14**, 499 (1995)
11. Benzerga, A., Besson, J.J., Pineau, A.: Anisotropic ductile fracture. Part II: theory. Acta Mater. **52**, 4639 (2004)
12. Cazacu, O., Stewart, J.: Analytic plastic potential for porous aggregates with matrix exhibiting tension–compression asymmetry. J. Mech. Phys. Solids **57**, 325 (2009)
13. Stewart, J., Cazacu, O.: Analytical yield criterion for an anisotropic material containing spherical voids and exhibiting tension-compression asymmetry. Int. J. Solids Struct. **48**, 357 (2011)
14. Benallal, A., Desmorat, R., Fournage, M.: An assessment of the role of the third stress invariant in the Gurson approach for ductile fracture. Eur. J. Mech. A Solids **47**, 400 (2014)
15. Vadillo, G., Reboul, J., Fernández-Sáez, J.: A modified Gurson model to account for the influence of the Lode parameter at high triaxialities. Eur. J. Mech. A Solids **56**, 31 (2016)
16. Perrin, G.: Homogenized behavior equations for porous Bingham viscoplastic material. J. Eng. Mech. **128**, 885 (2002)
17. Ponte-Castañeda, P.: The effective mechanical properties of nonlinear isotropic composites. J. Mech. Phys. Solids **39**, 45 (1991)
18. Willis, J.: On methods for bounding the overall properties of nonlinear composites. J. Mech. Phys. Solids **39**, 73 (1991)
19. Ponte-Castañeda, P., Zaidman, M.: Constitutive models for porous materials with evolving microstructure. J. Mech. Phys. Solids **42**, 1459 (1994)
20. Danas, K., Idiart, M., Ponte-Castañeda, P.: A homogenization-based constitutive model for isotropic viscoplastic porous media. Int. J. Solids Struct. **45**, 3392 (2008)
21. Idiart, M.: The macroscopic behavior of power-law and ideally plastic materials with elliptical distribution of porosity. Mech. Res. Commun. **35**(8), 583 (2008)
22. Leblond, J., Perrin, G., Suquet, P.: Exact results and approximate models for porous viscoplastic solids. Int. J. Plast. **10**(3), 213 (1994)
23. Gărăjeu, M., Michel, M.J., Suquet, P.: A micromechanical approach of damage in viscoplastic materials by evolution in size shape and distribution of voids. Comput. Methods Appl. Mech. Eng. **183**, 223 (2000)
24. Koplik, J., Needleman, A.: Void growth and coalescence in porous plastic solids. Int. J. Solids Struct. **24**, 835 (1988)
25. Brocks, W., Sun, D.Z., Hönig, A.: Verification of the transferability of micromechanical parameters by cell model calculations with visco-plastic materials. Int. J. Plast. **11**, 971 (1995)
26. Steglich, D., Brocks, W.: Micromechanical modelling of the behaviour of ductile materials including particles. Comput. Mater. Sci. **9**, 7 (1997)
27. Faleskog, J., Shih, C.: Micromechanics of coalescence I. Synergistic effects of elasticity, plastic yielding and multi-size-scale voids. J. Mech. Phys. Solids **45**, 21 (1997)
28. Fabrégue, D., Pardoen, T.: A constitutive model for elastoplastic solids containing primary and secondary voids. J. Mech. Phys. Solids **56**, 719 (2008)
29. Fritzen, F., Forest, S., Böhlke, T., Kondo, D., Kanit, T.: Computational homogenization of elasto-plastic porous metals. Int. J. Plast. **29**, 102 (2012)
30. Keralavarma, S., Hoelscher, S., Benzerga, A.: Void growth and coalescence in anisotropic plastic solids. Int. J. Solids Struct. **48**, 1696 (2011)
31. Gao, X., Kim, J.: Modeling of ductile fracture: significance of void coalescence. Int. J. Solids Struct. **43**, 6277 (2006)
32. Tvergaard, V.: Behaviour of voids in a shear field. Int. J. Fract. **158**, 41 (2009)
33. Scheyvaerts, F., Onck, P., Tekoglu, C., Pardoen, T.: The growth and coalescence of ellipsoidal voids in plane strain under combined shear and tension. J. Mech. Phys. Solids **59**, 373 (2011)
34. Srivastava, A., Needleman, A.: Porosity evolution in a creeping single crystal. Model. Simul. Mater. Sci. Eng. **20**, 035010 (2012)
35. Faleskog, J., Gao, X., Shih, C.: Cell model for nonlinear fracture analysis I. Micromech. Calibration Int. J. Fract. **89**, 355 (1998)

36. Gao, X., Faleskog, J., Shih, C.F.: Ductile tearing in part-through cracks: experiments and cell-model predictions. Eng. Fract. Mech. **59**, 761 (1998)
37. Lecarme, L., Tekoğlu, C., Pardoen, T.: Void growth and coalescence in ductile solids with stage III and stage IV strain hardening. Int. J. Plast. **27**, 1203 (2011)
38. ABAQUS/Standard, Simulia, User's Manual, version 6.15 edn. Dassault Systèmes, Providence (2015)
39. Kim, J., Gao, X., Srivatsan, T.S.: Modeling of void growth in ductile solids: effects of stress triaxiality and initial porosity. Eng. Fract. Mech. **71**, 379 (2004)
40. Vadillo, G., Fernández-Sáez, J.: An analysis of Gurson model with parameters dependent on triaxiality based on unitary cells. Eur. J. Mech. A Solids **28**, 417 (2009)
41. Gosh, A.: Tensile instability and necking in materials with strain hardening and strain-rate hardening. Acta Metall. **25**, 1413 (1977)
42. Klöcker, H., Tvergaard, V.: Growth and coalescence of non-spherical voids in metals deformed at elevated temperature. Int. J. Mech. Sci. **40**, 1995 (2003)
43. Vadillo, G., Zaera, R., Fernández-Sáez, J.: Consistent integration of the constitutive equations of Gurson materials under adiabatic conditions. Comput. Methods Appl. Mech. Eng. **197**, 1280 (2008)